43. J. Cohen, *Educ. Psychol. Meas.* **20**, 37 (1960).
44. E. J. Bromet, L. Dunn, M. M. Connell, M. A. Dew, H. C. Schulberg, *Arch. Gen. Psychiatr.* **43**, 435 (1986); A. E. Pulver and W. T. Carpenter, *Schizophr. Bull.* **9** (no. 3), 377 (1983).
45. V. Kraus, *Memagot.* **26**, 283 (1981).
46. M. A. Hidiroglou, W. A. Fuller, R. D. Hickman, *SuperCarp* (Iowa State Univ. Statistical Library, Ames, 1980).
47. W. A. Fuller, *Sankhya O.* **37**, 117 (1975).
48. A. W. Loranger, *Arch. Gen. Psychiatr.* **41**, 157 (1984).
49. H. Häfner *et al.*, *Psychol. Med.* **19**, 903 (1989).
50. E. F. Torrey, *Schizophr. Bull.* **17**, 15 (1991).
51. E. S. Paykel, in *Stressful Life Events: Their Nature and Effects*, B. S. Dohrenwend and B. P. Dohrenwend, Eds. (Wiley, New York, 1974), pp. 135–149.
52. G. W. Brown and T. Harris, *Social Origins of Depression* (Free Press, New York, 1978).
53. I. Levav, N. Zilber, E. Danielovich, E. Aisenberg, N. Turetsky, *Acta Psychiatr. Scand.* **75**, 183 (1987).
54. M. G. Marmot, M. Kogevanas, M. A. Elston, *Annu. Rev. Public Health* **8**, 111 (1987).
55. Supported by NIMH Research Grant MH30710, NIMH Clinical Research Center Grant 30906, NIMH Research Scientist Award MH14663, and the National Alliance for Research on Schizophrenia and Depression. We would like to acknowledge the invaluable collaboration with Israeli colleagues I. Rosenblum, E. Aisenberg, N. Turetsky, J. Magnes, and R. Lerer, and to thank various Israeli organizations and agencies for their generous cooperation: Public Opinion Research Institute of Israel (PORI), Israel Psychiatric Case Register, Israel Population Register, Israel Defense Forces, and Israel's psychiatric institutions and social welfare agencies. A number of Israeli researchers provided valuable assistance and advice, especially Z. Solomon, V. Kraus, S. Smooha, Y. Peres, E. Ben Raphael, and S. Yavetz. We would like to thank L. Erlenmeyer-Kimling for consultation on genetic factors and to express our appreciation to M. Reiff for computer assistance. A number of colleagues provided valuable criticisms at various drafts of this article: H. Häfner, D. Klein, N. Kreitman, D. Mechanic, M. Rutter, and anonymous reviewers. The late Dr. Barbara Snell Dohrenwend had a major influence on this study; this paper is dedicated to her memory.

Ozone Depletion: Ultraviolet Radiation and Phytoplankton Biology in Antarctic Waters

R. C. SMITH, B. B. PRÉZELIN, K. S. BAKER, R. R. BIDIGARE, N. P. BOUCHER, T. COLEY, D. KARENTZ, S. MACINTYRE, H. A. MATLICK, D. MENZIES, M. ONDRUSEK, Z. WAN, K. J. WATERS

The springtime stratospheric ozone (O_3) layer over the Antarctic is thinning by as much as 50 percent, resulting in increased midultraviolet (UVB) radiation reaching the surface of the Southern Ocean. There is concern that phytoplankton communities confined to near-surface waters of the marginal ice zone will be harmed by increased UVB irradiance penetrating the ocean surface, thereby altering the dynamics of Antarctic marine ecosystems. Results from a 6-week cruise (Icecolors) in the marginal ice zone of the Bellingshausen Sea in austral spring of 1990 indicated that as the O_3 layer thinned: (i) sea surface– and depth-dependent ratios of UVB irradiance (280 to 320 nanometers) to total irradiance (280 to 700 nanometers) increased and (ii) UVB inhibition of photosynthesis increased. These and other Icecolors findings suggest that O_3-dependent shifts of in-water spectral irradiances alter the balance of spectrally dependent phytoplankton processes, including photoinhibition, photoreactivation, photoprotection, and photosynthesis. A minimum 6 to 12 percent reduction in primary production associated with O_3 depletion was estimated for the duration of the cruise.

HUMAN ACTIVITIES, INCLUDING THE PRODUCTION OF chlorofluorocarbons, have reduced the concentration of stratospheric O_3 (*1–3*). The most dramatic loss of O_3 has been observed over Antarctica during the austral spring, where a 50% reduction in O_3—the widely discussed ozone hole—has been documented (*4–7*). Further reduction in average global stratospheric O_3 at all latitudes is predicted over the next century despite international efforts to address the problem (*8*). Reduced stratospheric O_3 results in increased flux of biologically damaging midultraviolet radiation (UVB, 280 to 320 nm) (*9–12*) to the surface of the earth and to ecologically significant depths in the ocean (*13–17*). Consequently, it has been hypothesized (*16, 18–24*) that marine life in the upper portion of the photic zone may be adversely affected by O_3-dependent increases in UVB radiation. Experimental evidence shows that exposure to UVB radiation decreases algal productivity (*19, 25–28*) and causes damage to various forms of aquatic larvae and other organisms (*29–37*). Furthermore, evidence suggests that environmentally relevant levels of UVB radiation now incident at the surface of the ocean should negatively impact various natural populations of marine organisms (*22, 33*). In spite of the mounting evidence, the extrapolation of these findings to allow prediction of impacts on the dynamics and vitality of natural, mixed communities of marine organisms is uncertain (*10, 11, 38–42*), and estimated impacts to the Antarctic marine ecosystem have ranged from insignificant to catastrophic (*43–45*).

Phytoplankton blooms in the Antarctic marginal ice zone (MIZ) are believed to contribute significantly to the overall productivity of the Southern Ocean throughout the austral spring and summer

R. C. Smith, S. MacIntyre, D. Menzies, Z. Wan, and K. J. Waters are with the Department of Geography and the University of California Marine Bio-Optics and the Computer Systems Laboratory–Center for Remote Sensing and Environmental Optics, University of California, Santa Barbara, CA 93106. B. B. Prézelin, N. P. Boucher, and H. A. Matlick are with the Department of Biological Sciences and the Marine Science Institute, University of California, Santa Barbara, CA 93106. K. S. Baker is with the University of California Marine Bio-Optics and the Scripps Institution of Oceanography, University of California at San Diego, La Jolla, CA 92093. R. R. Bidigare and M. Ondrusek are with the Department of Oceanography, University of Hawaii, Honolulu, HI 96822. T. Coley is with the Moss Landing Marine Labs, Moss Landing, CA 95039. D. Karentz is with the Laboratory of Radiobiology and Environmental Health, University of California, San Francisco, CA 94143-0750.

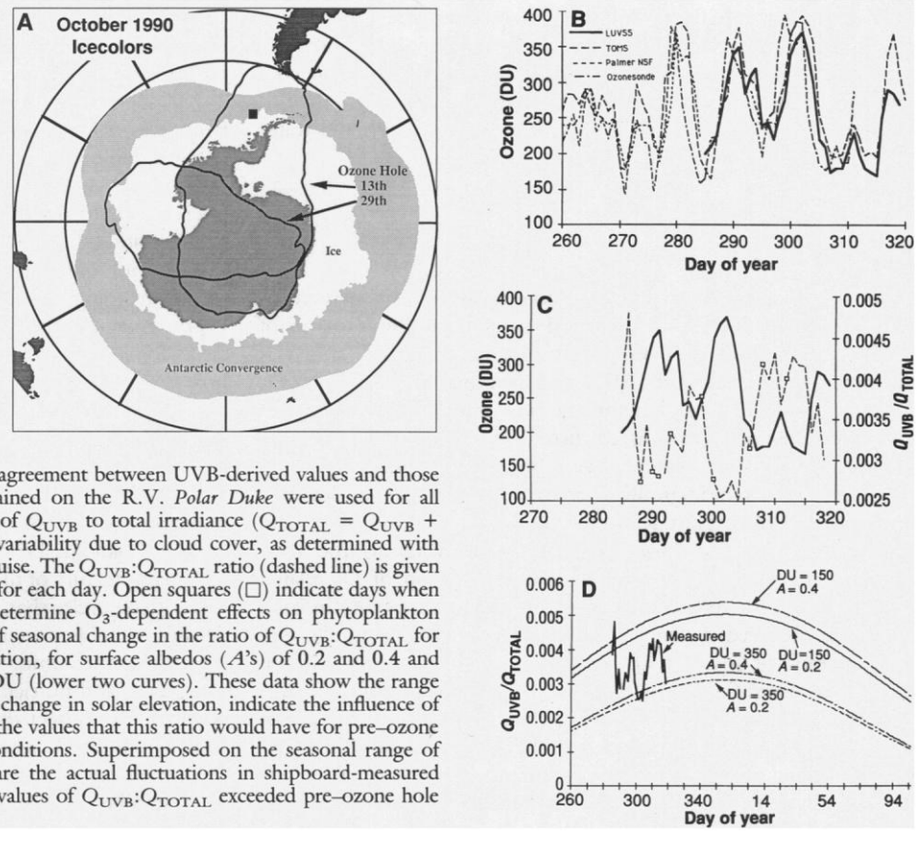

Fig. 1. (**A**) Ozone hole positions (depicted by 200-DU contours) with respect to the Antarctic continent (dark area) for 13 and 29 October 1990. The position of the pack ice (light area), the edge of the MIZ (outer edge of the light area) during the Icecolors '90 cruise, and the mean position of the Antarctic convergence within the Southern Ocean (outer edge of the gray area) are also shown. Cruise location, centered about 64°S 72°W, is indicated by the black box. (**B**) Ozone concentration (DU) versus time (day of year) for Palmer station and for the Icecolors '90 sampling area during austral spring 1990. Solid line gives values derived from UVB measurements on the R.V. *Polar Duke*. Dashed curves show values estimated from UVB measurements from the NSF monitoring station at Palmer, the O_3 values from balloon data taken at Palmer, and TOMS data for the Palmer sampling area (64°00′S, 72°30′W). The comparison shows the agreement between UVB-derived values and those obtained by balloon and by satellite. Data obtained on the R.V. *Polar Duke* were used for all computations discussed in the article. (**C**) Ratio of Q_{UVB} to total irradiance ($Q_{TOTAL} = Q_{UVB} + Q_{UVA} + Q_{PAR}$) at the ocean surface, including variability due to cloud cover, as determined with shipboard observations during the Icecolors '90 cruise. The Q_{UVB}:Q_{TOTAL} ratio (dashed line) is given for a 4-hour time interval centered on local noon for each day. Open squares (□) indicate days when in situ biological moorings were deployed to determine O_3-dependent effects on phytoplankton vitality. (**D**) A comparison of predicted patterns of seasonal change in the ratio of Q_{UVB}:Q_{TOTAL} for local noon and clear sky conditions at Palmer station, for surface albedos (*A*'s) of 0.2 and 0.4 and column O_3 of 150 (upper two curves) and 350 DU (lower two curves). These data show the range of natural variability in this ratio due to seasonal change in solar elevation, indicate the influence of the O_3 hole on this natural variability, and show the values that this ratio would have for pre–ozone hole, high albedo, clear sky, and midsummer conditions. Superimposed on the seasonal range of possible O_3-dependent variability in this ratio are the actual fluctuations in shipboard-measured Q_{UVB}:Q_{TOTAL} (solid curve). Early spring 1990 values of Q_{UVB}:Q_{TOTAL} exceeded pre–ozone hole maximum values over one-half of the time.

(*46–51*). With rapidly increasing insolation in the spring, the ice melts, forming a highly stable, relatively fresh, upper mixed layer over saltier deeper water. The resulting strong vertical stratification concentrates and restricts algal blooms to the near-surface waters of the MIZ, and these blooms proceed southward as the ice edge recedes, whereas the seaward edge of the bloom is diluted by wind processes that lead to mixing at deep levels (*47–56*). This stability within the MIZ, while permitting the phytoplankton to remain in the upper layers where there is sunlight and nutrients, also potentially restricts the growing phytoplankton to depths where UVB has increased significantly in areas beneath the O_3 hole. We carried out a 6-week cruise (Icecolors '90) in the MIZ of the Bellingshausen Sea (Fig. 1A) during a time of maximum O_3 depletion in order to test whether Antarctic pelagic phytoplankton communities are adversely influenced by O_3 depletion.

Atmospheric O_3 is a strong selective absorber of ultraviolet (UV) radiation (*57*). The shortest and most damaging UV wavelengths, UVC (200 to 280 nm), are absorbed strongly by the atmosphere so that negligible amounts reach the earth's surface. UVB is also extremely injurious to organisms, and it is this radiation that increases most significantly when stratospheric O_3 is reduced. The longest wavelengths of ultraviolet radiation (UVA, 320 to 400 nm) are known to induce both photodamage and photoreactivation processes in living cells (*38, 58–60*), and this radiation is relatively unaffected by variations in stratospheric O_3 concentrations. Photosynthetically available radiation (PAR, 400 to 700 nm), like UVA, is nearly independent of O_3 concentration. As a consequence, stratospheric O_3 depletion leads to a dramatic increase in damaging UVB irradiance, Q_{UVB}, whereas the corresponding irradiance in the UVA, Q_{UVA}, and in the PAR, Q_{PAR}, remain relatively constant.

A knowledge of Q_{UVB} incident at the ocean surface and of the depth and magnitude of its penetration, as well as an estimate of the time spent by the phytoplankton at depth, is required to determine the irradiance or dose rate to which in situ phytoplankton communities are exposed to UVB radiation over different time and space scales (*15, 28, 61–63*). Such information is required for quantification of the damage to phytoplankton as a function of the magnitude and duration of O_3-dependent UVB exposure in underwater light fields. The biological weighting function for phytoplankton damage is poorly understood and is the subject of active research. We designed our experiment to measure the differential effects on phytoplankton inside and outside the area beneath the O_3 hole, effects that we show are measurable in spite of our ignorance of an appropriate biological weighting function. We used a new in-water UV spectroradiometer to determine the penetration of UV radiation into Antarctic waters and a newly designed incubation system to quantify the impact of UVB radiation on phytoplankton pigmentation, photosynthetic physiology, growth processes, and overall rates of springtime primary productivity in the MIZ of the Bellingshausen Sea. The dynamics of the O_3 hole (Fig. 1A) produce a sharp atmospheric gradient in O_3, thus creating a Q_{UVB} front analogous to an oceanographic front in which the boundary is constantly repositioned by physical forcing functions (*41, 42*). The ratio of Q_{UVB} to total irradiance (Q_{TOTAL}) is significantly greater inside than outside the hole (Fig. 1, B, C, and D).

Our sampling strategy was designed to encompass a representative area of the MIZ in the Southern Ocean that would experience a significant variability in the concentrations of O_3 above the ship's location (Fig. 1, A, B, and C). During a 6-week period (September to November 1990) we carried out four north-south (each ~280 km) and three east-west (each ~72 km) transects of intensive vertical profiling (*64–67*) to define the physical, optical, chemical, and biological characteristics of the MIZ. At selected stations in the MIZ we made intensive observations to document the influence of increased UVB radiation on phytoplankton. In addition, we made a relatively long east-west transect from 80°W to

64°W within the MIZ (~860 km) to broaden the longitudinal extent of our observations. A new light and ultraviolet submersible spectroradiometer (LUVSS), capable of measuring full spectral irradiance and underwater radiance to high resolution, was used to determine the penetration of UV as a function of depth and water type (Fig. 2).

Results and Discussion

Four replicate hydrographic and bio-optical transects perpendicular to the ice edge allowed us to identify and follow the area of maximum phytoplankton productivity in the MIZ. The ship was positioned in this area of the MIZ, and the impact of fluctuating O_3 concentration on natural phytoplankton communities was quantified. Downwelling spectral irradiance (250 to 750 nm) incident at the ocean surface was monitored every minute at the ship's location. Recognizing that biologically effective solar radiation varies over several orders of magnitude with solar elevation, cloud cover, and depth, we often normalized spectral components to the total irradiance. This permits a quantitative comparison of O_3-related changes in UVB over the wide range of natural variability in solar irradiance observed. From the full spectral data (for example, Fig. 2A), the ratio of Q_{UVB} to Q_{TOTAL} ($Q_{TOTAL} = Q_{UVB} + Q_{UVA} + Q_{PAR}$) was determined (Fig. 1, B and C), and total column O_3 was estimated with a complete radiative transfer model of the atmosphere (*68*). The in-water measurements are consistent with previous work, and the O_3 estimates compare well with Total Ozone Mapping System (TOMS) satellite estimates (*69*), Palmer balloon data (*70*), and surface data from the Palmer National Science Foundation Monitoring Station (*71*). During this 6-week period, O_3 concentrations and the corresponding noontime Q_{UVB}:Q_{TOTAL} ratios varied by more than a factor of 2. As a consequence, phytoplankton experienced enhanced Q_{UVB} during most of the spring, modulated by the movement of the O_3 hole. The springtime Q_{UVB}:Q_{TOTAL} ratio within the hole [~150 Dobson units (DU)] is larger than would ever exist, even at summer solstice, under normal (~350 DU) O_3 concentrations (Fig. 1D) (*72*).

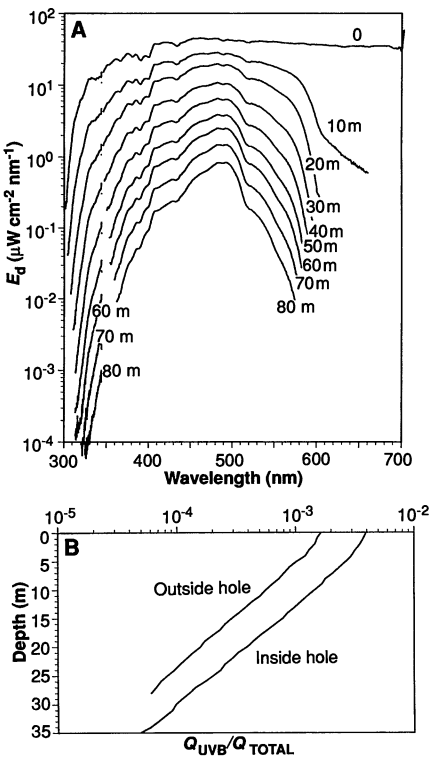

Fig. 2. (**A**) Downwelling spectral irradiance E_d versus wavelength for selected depths as measured with the LUVSS instrument. This instrument has 0.2-nm resolution from 250 to 350 nm and 0.8-nm resolution from 350 to 700 nm. It is deployed by a remote operating vehicle that allows accurate in-water data to be obtained independent of ship perturbation effects (*107–109*). Above-surface and in-water spectra are measured simultaneously to allow for full spectral correction of the in-water data for variability in sun angle and clouds (*73, 74*). (**B**) Depth versus the ratio of Q_{UVB}:Q_{TOTAL} for MIZ area for a day inside (1 October 90) and outside (28 October 90) the O_3 hole. The O_3 hole increases the effective penetration depth of UVB radiation by about 7 m.

Full spectral irradiance, including the UVB region of the spectrum, was determined as a function of depth at the stations where detailed biological observations were carried out (Fig. 2A). The methods of Smith and Baker (*73, 74*) allow the spectral diffuse attenuation coefficient $K(z, \lambda)$, biological effective dose rates (*15*), and the ratio Q_{UVB}:Q_{TOTAL} to be estimated from these in-water data as a function of depth (z) and wavelength (λ) (Fig. 2B) for comparison with biological observations. Whereas the Q_{UVB}:Q_{TOTAL} ratio is O_3-dependent in the Southern Ocean, the vertical attenuation coefficients for spectral irradiance are nearly the same in and out of the O_3 hole (Fig. 2B). Therefore, if Q_{UVB} is doubled at the surface, it will be doubled at all depths, and the critical depth for UVB damage effects will be deeper in the water column. We found that UV penetrates to ecologically significant depths, a result consistent with earlier work (*17*). The new LUVSS was sufficiently sensitive to detect UVB radiation at depths in excess of 60 to 70 m, well below depths where we noted biological effects on rates of primary production.

A major feature of the MIZ is the presence of ice, which, through freeze-thaw cycles that change the surface layer's salinity and hence density, is an important factor in establishing the stability of the upper water column. Figure 3 shows the hydrography, optical properties, and nutrient and pigment distributions for our second north-south transect through the MIZ. The data show that mesoscale variations occurred over time scales of days. During springtime, meltwater creates density gradients that promote water column stability and subsequent phytoplankton growth (*75*). The contours of salinity and density (σ_t) show that the mixed-layer depth (MLD) generally increased with distance from the pack ice and was influenced primarily by an increasingly thick lens of fresher water and greater wind mixing away from the pack ice (Fig. 3, A through C). The MIZ is dynamic and can change rapidly in response to physical forcing events, including diurnal variability of solar insolation, leading to increased stratification during daylight followed by convective overturning at night. We infer from these and other data that the depth of surface mixing progressively shallowed near the edge of the pack ice and that relatively stable water columns characterized stations where phytoplankton biomass was elevated. Finer scale temperature profiles and corresponding profiles of σ_t (not shown) often indicated near-surface inversions and provided estimates of centimeter- to meter-scale vertical movement occurring on time scales of minutes to hours within the stably stratified water near the pack ice.

Inorganic nutrient concentrations (Fig. 3, E, F, and K) were high, and phytoplankton growth was presumably limited by light, not nutrient, availability (*76*). However, nutrient concentrations were variable, suggesting that some physical mixing was occurring (stations 26 and 27) and that plants were using nutrients for growth (stations 23, 24, 30, and 31). The quantity chlorophyll a, a measure of phytoplankton biomass, was highest near the edge of the pack ice and at station 24 (Fig. 3H). The beam attenuation coefficient (Fig. 3G) is a measure of suspended particulate matter and was highly correlated with chlorophyll a distributions, suggesting that the suspended particles sampled in our study region were dominated by living phytoplankton. The prymnesiophyte *Phaeocystis* spp. dominated most phytoplankton communities, as has been observed on occasion for these Antarctic waters (*77–79*), and cell densities ranged from 1000 to 4000 cells per milliliter. The remainder of the phytoplankton communities consisted mostly of diatoms (30 to 400 cells per milliliter). An excellent correspondence (data not shown) was observed between microscopically enumerated phytoplankton counts (*Phaeocystis* spp. and diatoms) and distributions of their

respective diagnostic pigments 19′-hexanoyloxyfucoxanthin (Fig. 3I) and fucoxanthin (Fig. 3J). Very low concentrations of dinoflagellates (less than one cell per milliliter) were observed in plankton samples. The low and variable concentrations of chlorophyll b and alloxanthin measured along the transect line revealed that green algae and cryptophytes were only minor phytoplankton biomass components (data not shown).

Phytoplankton have a number of photoreactivation and photoprotective strategies to partially compensate for photoinhibitory effects of different wavelengths of light (*80–82*). During Icecolors '90, we attempted to elucidate these strategies by determining (i) the impact of UV radiation on the growth potential of two isolated clones of Antarctic phytoplankton; (ii) the potential lethality of UVB radiation on unprotected microbes; (iii) the presence of UV photoprotectants in the water column; and (iv) the distribution of UVA+PAR-photoprotective carotenoids in MIZ phytoplankton communities. The results of the first study (Fig. 4) indicated that the UVB inhibition of growth rate was much greater for a *Phaeocystis* spp. than for a clone of the diatom *Chaetoceros socialis*. Results indicate the vulnerability of *Phaeocystis* to decreasing stratospheric O_3 levels and demonstrate the species-specific nature of UVB inhibition that has been already demonstrated for laboratory cultures of Antarctic diatoms (*83, 84*). In the second study, sealed samples of a test bacterium with no means of DNA repair were incubated on the in situ productivity moorings and showed a lethality due to DNA damage that was directly related to O_3-dependent increases in Q_{UVB}. These results are similar to those reported for the 1988 Antarctic O_3 depletion (*85*). Analysis of our data suggests an ~3% loss of growing cells at 350 DU, compared with an estimated 25% loss at 200 DU. These dosimeter results represent an estimated upper limit for biological damage caused by UVB within the water column. Endemic microorganisms might use photoprotective strategies to mitigate UV effects to some extent. In our pigment studies, we documented an enhanced concentration of plant photoprotective carotenoids (diadinoxanthin, diatoxanthin, and β-carotene) in surface waters of the MIZ, and the presence of at least four different UV-absorbing, mycosporine-like amino acids (MAAs) was tentatively identified in filtered particle samples (*86*). MAAs have been detected in macroalgae, phytoplankton, and invertebrates (*87–90*), they absorb strongly between 270 and 350 nm, and cellular concentrations typically accumulate under high light conditions (*88, 91, 92*); thus, it is surmised that they function as photoregulated UV blockers for marine algae and invertebrates.

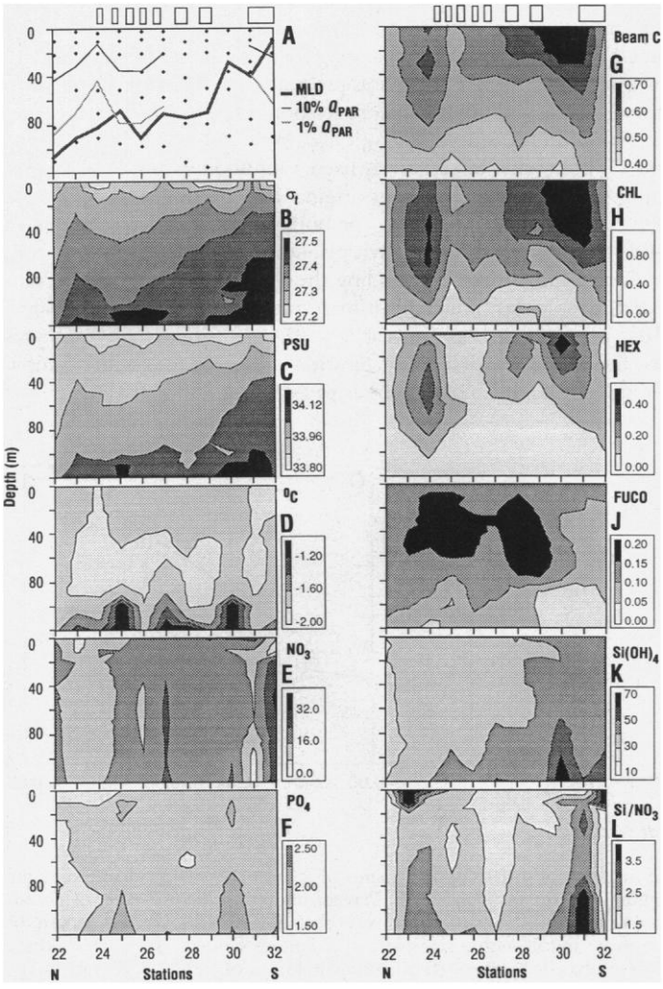

Fig. 3. North-south transect (stations 22 to 32 spaced at 12–nautical mile intervals; the transect required 24 hours to complete) through the MIZ. Stations 22 to 24 were in open water, 25 to 29 were in a transition zone from open water to close ice, and 30 to 32 were in increasingly dense pack ice. Hydrography [temperature (°C), salinity (PSU), density (σ_t), mixed layer depth (MLD)] and optics [% Q_{PAR}, beam attenuation coefficient at 660 nm (Beam C, m^{-1})] were continuously recorded as a function of depth. Black circles in (A) indicate discrete sampling depths for nutrients {nitrate (NO_3), phosphate (PO_4), silicate [$Si(OH)_4$]}, pigments [chlorophyll a (CHL), 19′-hexanoyloxyfucoxanthin (HEX), fucoxanthin (FUCO)], and the ratio of silicate to nitrate (Si/NO_3) versus depth (m) along north-south transect across the MIZ. The small boxes at the top schematically illustrate ice cover (*110*).

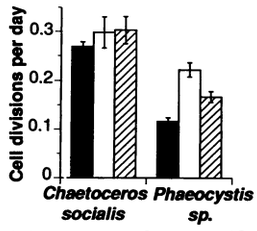

Fig. 4. Cell division rates for *Chaetoceros socialis* and *Phaeocystis* sp. under partitioned solar light regimes as described in Fig. 5 (solid bar, UVA + UVB + PAR; open bar, UVA + PAR; crosshatched bar, PAR). A deck system similar to MATWINGS provided 32 incubation slots per light treatment, where the natural illumination was attenuated with neutral-density screening. Differences in the three light treatments (UVT, Mylar, UF3; see Fig. 5 for description) provided the measure of UV-specific effects on growth rates of unialgal cultures of Antarctic phytoplankton. Initial (day 0) and final (day 9) cell densities were enumerated by epifluorescence to calculate division rates (cell doublings per day).

The stations where *Phaeocystis* spp. dominated (including station 30 of the north-south transect in Fig. 3) were selected for intensive biological sampling to test the influence of variable UV on the productivity of the most abundant phytoplankton communities of the MIZ. Primary productivity was shown to be inhibited by increased levels of both Q_{UVB} and Q_{UVA}, which we evaluated separately in order to assess specifically the influence of the O_3 hole (Fig. 5). Our study was designed to measure the differential effects of UV radiation on phytoplankton inside and outside the O_3 hole. We estimated the influence of UV radiation on in situ primary production by comparing three radiation treatments so that

$$P_{Q_{TOT}} = P_{Q_{PAR}}(1 - FI_{UVA} - FI_{UVB}) \quad (1)$$

where $P_{Q_{PAR}}$ is the rate of primary production for plants exposed to PAR only (natural radiation filtered so as to pass only 400 to 700 nm), $P_{Q_{TOT}}$ is the rate of primary production for plants exposed to unfiltered radiation (PAR + Q_{UVA} + Q_{UVB}), and FI_{UVA} and FI_{UVB} represent the fractional inhibition of primary production attributable to Q_{UVA} and Q_{UVB}, respectively. The fractional inhibition due to UVA radiation was determined as a function of UVA exposure ($Q_{UVA}t$, t = time) (Fig. 5A), UVB exposure ($Q_{UVB}t$) (Fig. 5B), and UVB exposure normalized to Q_{TOTAL} (Fig. 5C). A fit to these data can be used to estimate FI_{UVA} and FI_{UVB}, which when inserted in Eq. 1 allows an estimation of $P_{Q_{TOT}}$.

With our means of detection, O_3-related UVB inhibition of photosynthesis was evident in samples incubated down to depths of 25 m (the 4% Q_{PAR} level) (Fig. 5, B and C). UVB inhibition was determined as the ratio of productivity under total irradiance (Q_{TOTAL}) to productivity with Q_{UVB} excluded. Results indicate that UVB inhibition of photosynthesis increases linearly (within the accuracy of measurement) with increasing UVB dose (Fig. 5B) and with O_3-dependent increases in the ratio of Q_{UVB}:Q_{TOTAL} (Fig. 5C). As above, we used normalized spectral ratios so as to focus on O_3-related, rather than sun angle– and cloud-related, variability. The rate constants for UVB inhibition differed for surface and subsurface phytoplankton communities. As the UVB dose and the ratio of ($Q_{UVB}t$):(Q_{TOTAL}) increased, surface samples displayed a residual 15 to 20% UVB inhibition of photosynthesis by the end of a 7- to 12-hour incubation, compared to 40 to 60% for samples from a depth of 5 m. Furthermore, transfer experiments (not shown), in which samples taken from depth were incubated at the surface and vice versa, showed that UVB inhibition effects are independent of the sample depth and depend only on dose at the depth incubated. For instance, 5-m samples moved to surface conditions displayed UVB inhibition effects by the end of the day that were characteristic of surface samples and much lower than those of 5-m controls. When compared with results of shorter term experiments (not shown), the combined findings strongly suggest that (i) UVB inhibition of surface samples may be greatest during morning hours and mitigated by photoprotective mechanisms photoinduced during the day; and (ii) UVA photoregulation of UVB photoprotective mechanisms may largely control the pattern of UVB inhibition of primary production in the MIZ.

Figure 6 represents a working model that is consistent with Icecolors observations of the effects of Q_{UVB}, Q_{UVA}, and Q_{PAR} on primary productivity and DNA integrity for phytoplankton communities of the Antarctic MIZ. Although this working model is consistent with our experimental results, the causes of the depth-related variations in UVB inhibition remain uncertain and are the subject of further investigations. Most pathways shown are known (*93, 94*), whereas the UVA photoregulation of cell responses to UVB radiation was deduced and is here proposed as the simplest mechanism to account for the subsurface maximum in UVB inhibition of rates of primary production. In this model, Q_{UVB}, Q_{UVA}, and Q_{PAR} act differentially to damage DNA integrity and photosynthetic processes. The rate of cell damage by these light-dependent processes may be offset by the rates of UVA+PAR–dependent photoreactivation, UV absorption by photoprotective MAAs, high-irradiance PAR induction of photoprotective carotenoids, and light-independent ("dark") DNA repair processes. In this model, the differing UVB exposure-to-response curve for surface and subsurface samples (Fig. 5, B and C) is consistent with the hypothesis that the remediation of UVB damage to cell vitality is initiated through UVA, but not UVB, photoreceptors. Under this hypothesis, phytoplankton are cued to short-term (minutes to a few hours) changes in UVA flux as an index of changing total UV flux. The use of Q_{UVA} as a signal for repair and photoprotective capabilities would leave these phytoplankton unable to respond favorably to significant elevations in the ratio of Q_{UVB}:Q_{UVA} that, before the formation of the O_3 hole, had been relatively fixed. Our findings and this working model are consistent with our original hypothesis that the ratios of Q_{UVB}:Q_{UVA} or Q_{UVB}:Q_{PAR} or both are critical determinants of susceptibility of Antarctic phytoplankton to O_3 depletion.

For pelagic waters surrounding the MIZ of the Southern Ocean, current estimates of annual primary productivity are about 610 × 10^{12} grams of carbon per year (*76, 95, 96*). Productivity estimates for the MIZ were derived by Smith and Nelson (*48*) with a simple model of ice-edge bloom genesis to be about 380 × 10^{12} grams of

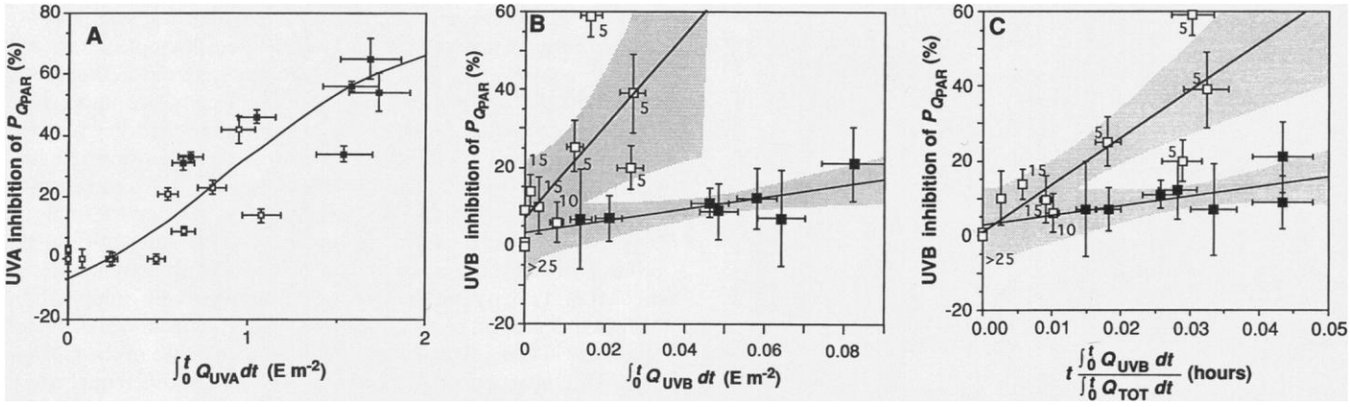

Fig. 5. The percent in situ UV inhibition of PAR rates of photosynthesis for the upper 40 m of the Antarctic MIZ in October to November 1990. BOPSII water samples were collected at discrete depths at dawn and inoculated with ^{14}C-radiolabeled sodium bicarbonate (*111*). Radioactive techniques and controls have been described (*111, 112*). Replicate aliquots (300 to 500 ml) were dispensed into Whirlpak bags and deployed in a specially designed spar buoy system (MATWINGS) in which three optically distinct incubation wings were attached at each depth to provide (UVA + UVB + PAR) (280 to 700 nm), (UVA + PAR) (320 to 700 nm), and PAR (400 to 700 nm) light treatments. These treatments were obtained by three plastic, sharp cutoff filters with half-transmittance points of 400 (UF3), 323 (Mylar), and 296 nm (UVT). Each wing held 12 productivity, pigment, actinometer, and dosimeter samples. The 17 different mooring incubations shown above began by midmorning and lasted 7 to 12 hours. The percent inhibition of PAR rates of photosynthesis by UVA and UVB radiation was separated and quantified by comparison of productivity rates in light treatments distinguished by the inclusion or exclusion of Q_{UVA} and Q_{UVB}. In-water exposure was calculated from LUVSS measurements of the spectral attenuation (280 to 700 nm) of the in-water light fields and 10-min averages of full spectral surface measurements of 280 to 700 nm irradiance over the duration of the incubation. (**A**) Percent inhibition of PAR rates of photosynthesis versus in situ Q_{UVA} exposure integrated over the length of exposure and fit with a sigmoid curve. Surface samples (■) were collected and incubated at <2 m. (**B**) Percent inhibition of PAR rates of photosynthesis versus in situ Q_{UVB} exposure integrated over the length of exposure. Linear regressions gave slopes for surface data (■) and subsurface data (□) of 154 ± 63 and 1181 ± 452, respectively. Depths of subsurface samples (□) are indicated in meters. The 90% confidence intervals for the regression lines are shown as the shaded area. Error bars represent an assumed maximum 10% error in irradiance data and the SD for four replicate productivity measurements. (**C**) Percent UVB inhibition of PAR rates of photosynthesis versus in situ UVB exposure integrated over the length of exposure and normalized to the integrated in situ Q_{TOTAL} for the same time period times the length of exposure. Linear regression gave slopes for surface data (■) and subsurface data (□) of 268 ± 164 and 1285 ± 265, respectively. The 90% confidence intervals for the regression lines are shown as the shaded area. Error bars represent an assumed maximum 10% error in light data and the SD for four replicate productivity measurements.

carbon per year or about 40% of the total MIZ plus pelagic production south of the Antarctic Convergence. Thus, the MIZ potentially has a major role in the ecological and biogeochemical cycles of the Southern Ocean.

Our data permit an estimate to be made of the impact of the O_3 hole on primary production for the MIZ of the Bellingshausen Sea. In situ production for moorings inside the O_3 hole (stratospheric O_3 levels less than 200 DU) can be directly compared with production for moorings outside the O_3 hole (greater than 300 DU) as a function of depth and independent of any assumptions with respect to processes involved in the depth-related experimental results. Comparison of integrated productivity versus depth curves, with excluded UVB (from outside the hole) and with included UVB (from inside the hole), consistently show that higher UVB levels are associated with reduced (6 to 12%) water column productivity. As discussed above, Q_{UVB} is dependent on O_3, solar elevation, and cloud conditions. The fitted relations between photosynthetic inhibition and Q_{UVB}:Q_{TOTAL} (Fig. 5C) permit an estimation of the impact of the O_3 hole, independent of solar elevation and cloud conditions, and a generalization of results to the MIZ of the Bellinghausen Sea (Fig. 7). From these fitted data, and with each curve applied to the appropriate depth, we find that the reduction in productivity of the MIZ caused by O_3 depletion is between 6 and 12%. This result is consistent with the above simple comparison of the productivity depth profiles inside and outside the O_3 hole.

On the basis of these in situ data, one can make a yearly estimate of production loss for the Southern Ocean by assuming that this loss is representative of the entire MIZ and integrating production over this area and over the 3-month duration of the O_3 hole during Antarctic spring. We estimate (using a 6% loss of water column productivity and conservatively assuming a given location is outside the O_3 hole one-half of the time) that this productivity loss to the MIZ is 7×10^{12} grams of carbon per year, corresponding to about 2% of the estimated yearly production of the MIZ. Our assumptions are such that this is a minimum loss estimate, and values could be at least twice these values depending on the specific space-time extent of the O_3 hole. We have used short-term ^{14}C studies to assess changes in natural communities of phytoplankton caused by variations in the O_3 hole that occurred on time scales from hours to weeks. Thus, the time scale of our experimental protocol matched that of the processes observed. Caution must be used when inferring longer term ecological consequences from short-term observations (*16*).

The interannual variability of primary production of the MIZ has been estimated to be substantial (*97*) and such that the maximum productivity is 50% greater than the minimum. This variability associated with the annual advance and retreat of pack ice is thought to be a major physical determinant of space-time changes in the structure and function of polar biota (*48, 98*). In particular, this interannual variability is likely to have a significant effect on total annual primary production, although to date these natural changes have not been accurately quantified. Thus, our estimated (2 to 4%) loss to MIZ productivity should be viewed in the context of a presumed natural variability of ±25%. Concern has been expressed (*44*) that O_3-induced phytoplankton loss may trigger a positive feedback with respect to atmospheric CO_2 that would exacerbate the greenhouse effect. Our estimated loss of 7×10^{12} grams of carbon per year is about three orders of magnitude smaller than estimates of global phytoplankton production and thus is not likely to be significant in this context. On the other hand, we find that the O_3-induced loss to a natural community of phytoplankton in the MIZ is measurable, and the subsequent ecological consequences of the magnitude and timing of this early spring loss remain to be determined.

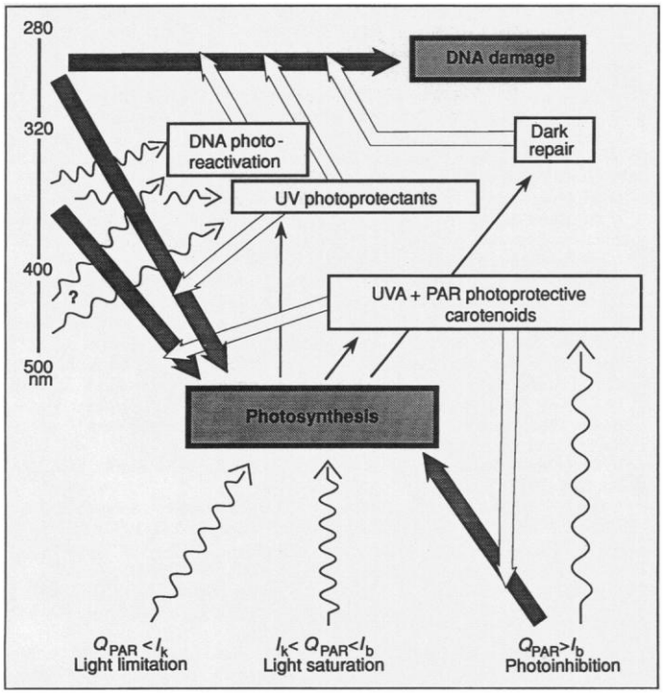

Fig. 6. A working model of the photoregulatory interactions of Q_{UVB}, Q_{UVA}, and Q_{PAR} on primary productivity and DNA integrity for phytoplankton communities of the Antarctic MIZ (see text for details). I_k is the saturation parameter for photosynthesis, and I_b is the photoinhibition onset parameter. Shaded arrow, known direct photoinhibitory effects on phytoplankton vitality by high fluxes of Q_{UVB}, Q_{UVA}, and Q_{PAR}; open arrow, known processes that diminish the photoinhibitory effects of Q_{UVB}, Q_{UVA}, and Q_{PAR}; wavy arrow, known light-mediated processes that regulate biosynthetic rates; straight arrow, known biosynthetic processes that regulate photoprotective processes; question mark, hypothesized pathways of photoregulation consistent with the database of Icecolors.

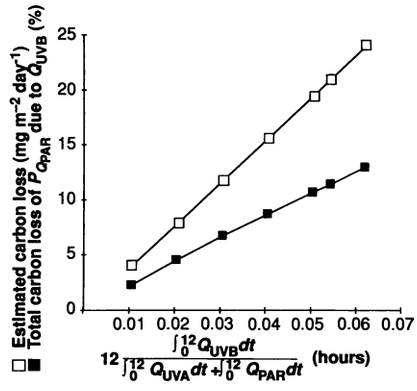

Fig. 7. An illustration of the impact of changing O_3 levels on the inhibition of integrated water-column primary productivity of phytoplankton communities in the upper 25 m of the Antarctic MIZ in October to November 1990. Using all mooring data for days when atmospheric O_3 levels were ~200 DU (Fig. 1, B and C), we determined the depth-dependent and integrated rates of production in the presence (inside the O_3 hole) and absence (outside the O_3 hole or by exclusion) of UVB radiation. Using these data in combination with the observed Q_{UVB}:Q_{TOTAL}–dependent rates of inhibition documented in Fig. 5C, we estimated absolute and percent total losses of primary production due to UVB radiation over a range of atmospheric O_3 concentrations. In this figure, values >0.05 are typical of exposures inside the O_3 hole, and values <0.025 are typical of exposures outside.

REFERENCES AND NOTES

1. R. Watson, *Ozone Trends Panel* (National Aeronautics and Space Administration, Washington, DC, 1988).
2. J. G. Anderson, D. W. Toohey, W. H. Brune, *Science* **251**, 39 (1991).
3. M. R. Schoeberl and D. L. Hartmann, *ibid.*, p. 46.
4. G. Brasseur, *Environment* **29**, 6 (1987).
5. S. Solomon, *Rev. Geophys.* **26**, 131 (1988).

6. _____, *Nature* **347**, 347 (1990).
7. J. E. Frederick and H. E. Snell, *Science* **241**, 438 (1988).
8. M. Crawford, *ibid.* **237**, 1557 (1987).
9. National Research Council, Committee on Impacts of Stratospheric Change, *Stratospheric Ozone Depletion by Halocarbons: Chemistry and Transport* (National Academy Press, Washington, DC, 1979).
10. National Research Council, Committee on Chemistry and Physics of Ozone Depletion and Committee on Biological Effects of Increased Solar Ultraviolet Radiation, *Causes and Effects of Stratospheric Ozone Reduction: an Update* (National Academy Press, Washington, DC, 1982).
11. National Research Council, Committee on Causes and Effects of Changes in Stratospheric Ozone, *Causes and Effects of Stratospheric Ozone Reduction: Update 1983* (National Academy Press, Washington, DC, 1984).
12. D. Lubin *et al.*, *J. Geophys. Res.*, in press.
13. N. G. Jerlov, *Nature* **166**, 111 (1950).
14. J. Lenoble, *Ann. Geophys.* **12**, 16 (1956).
15. R. C. Smith and K. S. Baker, *Photochem. Photobiol.* **29**, 311 (1979).
16. _____, *Science* **208**, 592 (1980).
17. _____, *Appl. Opt.* **20**, 177 (1981).
18. R. C. Worrest, H. Van Dyke, B. E. Thomson, *Photochem. Photobiol.* **17**, 471 (1978).
19. R. C. Worrest, D. L. Brooker, H. Van Dyke, *Limnol. Oceanogr.* **25**, 360 (1980).
20. R. C. Worrest *et al.*, *Photochem. Photobiol.* **33**, 223 (1981).
21. R. C. Smith, K. S. Baker, O. Holm-Hansen, R. Olson, *ibid.* **31**, 585 (1980).
22. J. Calkins and T. Thordardottir, *Nature* **283**, 563 (1980).
23. G. Dohler, *Mar. Biol.* **83**, 247 (1984).
24. D.-P. Häder and M. A. Häder, *Arch. Microbiol.* **150**, 20 (1988).
25. L. A. Hobson and F. A. Hartley, *J. Plankton Res.* **5**, 325 (1983).
26. P. L. Jokiel and R. H. York, *Limnol. Oceanogr.* **29**, 192 (1984).
27. H. Maske, *J. Plankton Res.* **6**, 351 (1984).
28. J. J. Cullen and M. P. Lesser, *Mar. Biol.* **111**, 183 (1991).
29. O. Siebeck, *Verh. Int. Ver. Limnol.* **20**, 2469 (1978).
30. J. J. Karanas, H. van Dyke, R. C. Worrest, *Limnol. Oceanogr.* **24**, 1103 (1979).
31. J. R. Hunter, J. H. Taylor, G. Moser, *Photochem. Photobiol.* **29**, 325 (1979).
32. D. M. Damkaer, D. B. Dey, G. A. Heron, *Oecologia (Berlin)* **48**, 178 (1981).
33. J. R. Hunter, S. E. Kaupp, J. H. Taylor, in *The Role of Solar Ultraviolet Radiation in Marine Ecosystems*, J. Calkins, Ed. (Plenum, New York, 1982), pp. 459–497.
34. D. M. Damkaer and D. B. Dey, *Oecologia* **60**, 169 (1983).
35. J. Ringelberg, A. L. Keyser, B. J. G. Flik, *Hydrobiologia* **112**, 217 (1984).
36. W. R. Jeffery, *Dev. Biol.* **140**, 388 (1990).
37. J. M. Shick, M. P. Lesser, W. R. Stochaj, *Symbiosis* **10**, 145 (1991).
38. M. M. Caldwell, L. B. Camp, C. W. Warner, S. D. Flint, in *Stratospheric Ozone Reduction, Solar Ultraviolet Radiation and Plant Life*, R. C. Worrest and M. M. Caldwell, Eds. (Springer-Verlag, Berlin, 1986), pp. 87–111.
39. R. C. Worrest, in *Effects of Changes in Stratospheric Ozone and Global Climate, Overview*, J. G. Titus, Ed. (U.S. Environmental Protection Agency and United Nations Environmental Program1, New York, 1986), pp. 175–191.
40. *Stratospheric Ozone: The State of the Science and NOAA's Current and Future Research* (National Oceanic and Atmospheric Administration, Washington, DC, 1987).
41. R. C. Smith, *Photochem. Photobiol.* **50**, 459 (1989).
42. _____ and K. S. Baker, *Oceanography* **2**, 4 (1989).
43. L. Roberts, *Science* **244**, 288 (1989).
44. M. A. Voytek, *Ambio* **19**, 52 (1990).
45. D. Karentz, *Antarct. Sci.* **3**, 3 (1991).
46. S. Z. El-Sayed, in *Biology of the Antarctic Seas IV*, G. A. Llano and I. E. Wallen, Eds. (1971 observations on phytoplankton blooms in the Weddel Sea), p. 301.
47. _____, in *Polar Research: To the Present, and the Future*, M. A. McWhinnie, Ed. (Westview, Boulder, CO, 1978), p. 141.
48. W. O. Smith, Jr., and D. M. Nelson, *BioScience* **36**, 251 (1986).
49. D. L. Wilson, W. O. Smith, Jr., D. M. Nelson, *Deep Sea Res.* **33**, 1375 (1986).
50. D. M. Nelson, W. O. Smith, Jr., L. I. Gordon, B. A. Huber, *J. Geophys. Res.* **92**, 7181 (1987).
51. D. M. Nelson *et al.*, *Deep Sea Res.* **36**, 191 (1989).
52. H. H. Gran, *Rapp. P.V. Reun. Cons. Int. Explor. Mer.* **75**, 37 (1931).
53. P. T. Marshall, *J. Cons. Cons. Int. Explor. Mer* **23**, 173 (1957).
54. H. J. Niebauer and V. Alexander, *Cont. Shelf Res.* **4**, 367 (1985).
55. W. O. Smith, Jr., and D. M. Nelson, in *Antarctic Nutrient Cycles and Food Webs*, W. R. Siegfried, P. R. Condy, R. M. Laws, Eds. (Springer-Verlag, Berlin, 1985), pp. 70–77.
56. _____, *Science* **227**, 163 (1985).
57. L. T. Molina and M. J. Molina, *J. Geophys. Res.* **91**, 14 (1986).
58. M. M. Caldwell, *Ecol. Monogr.* **38**, 243 (1968).
59. B. Buhlmann, P. Bossard, U. Uehlinger, *J. Plankton Res.* **9**, 935 (1987).
60. T. Hirosawa and S. Miyachi, *Arch. Microbiol.* **135**, 98 (1983).
61. H. J. Morowitz, *Science* **111**, 229 (1950).
62. R. G. Zepp and D. M. Cline, *Environ. Sci. Technol.* **11**, 359 (1977).
63. R. C. Smith and K. S. Baker, in *The Role of Solar Ultraviolet in Marine Ecosystems*, J. Calkins, Ed. (Plenum, New York, 1982), pp. 509–537.
64. A second-generation bio-optical profiling system BOPSII (*65*) was used to determine physical, optical, and biological properties of the MIZ. This instrument, with a 12-bottle rosette (51 GoFlo bottles) and a depth capability of 500 m, was the principle hydrographic and sampling instrument for the cruise. Properties measured by the new instrument included temperature, conductivity, depth, up- and downwelling spectral irradiance (410, 441, 488, 507, 520, 565, 589, and 625 nm), upwelled spectral radiance (410, 441, 488, 520, 565, 625, and 675 nm), downwelling scalar irradiance (410, 441, 488, 520, and 565 nm), beam transmittance (660 nm), stimulated chlorophyll fluorescence, in situ chlorophyl fluorescence, and PAR. In addition, an Ocean Sensors Model 100 conductivity, temperature, and depth device (CTD) with a depth resolution of 3 to 5 mm was used to measure temperature (±0.001°C) and conductivity (±0.001 m ohm cm^{-1}) fine structure to define the mixed layer and the mixing zones (*66, 67*) within the mixed layer.
65. R. C. Smith, C. R. Booth, J. L. Star, *Appl. Opt.* **23**, 2791 (1984).
66. S. A. Thorpe, *Philos. Trans. R. Soc. London Ser. A* **286**, 125 (1977).
67. T. M. Dillon, *J. Geophys. Res.* **87**, 9601 (1982).
68. R. C. Smith, Z. Wan, K. S. Baker, *ibid.*, in press.
69. A. Krueger, personal communication.
70. A. Torres, personal communication.
71. C. R. Booth, personal communication.
72. J. E. Frederick, H. E. Snell, E. K. Haywood, *Photochem. Photobiol.* **50**, 443 (1989).
73. R. C. Smith and K. S. Baker, *Proc. SPIE Ocean Opt. VII* **489**, 119 (1984).
74. _____, *Proc. SPIE Ocean Opt. VIII* **637**, 95 (1986).
75. W. O. Smith, Jr., *Oceanogr. Mar. Biol.* **25**, 11 (1987).
76. _____ and E. Sakshaug, *Polar Oceanography*, part B, *Chemistry, Biology, and Geology* (Academic Press, New York, 1990), pp. 427–525.
77. G. A. Fryxell, E. C. Theriot, K. R. Buck, *Antarct. J. U.S.* **19**, 107 (1984).
78. R. A. Perrin, P. Lu, H. J. Marchant, *Hydrobiologia* **146**, 33 (1987).
79. W. O. Smith, Jr., *et al.*, *Nature* **352**, 514 (1991).
80. A. W. D. Larkum and J. Barrett, *Adv. Bot. Res.* **10**, 1 (1983).
81. F. T. Haxo, *J. Phycol.* **21**, 282 (1985).
82. R. R. Bidigare, *Photochem. Photobiol.* **50**, 469 (1989).
83. D. Karentz, J. E. Cleaver, D. L. Mitchell, *Nature* **350**, 28 (1991).
84. _____, *J. Phycol.* **27**, 326 (1991).
85. D. Karentz and L. H. Lutze, *Limnol. Oceanogr.* **35**, 549 (1990).
86. During Icecolors '90, suspended particulate samples were screened for MAAs to assess their importance as UV blockers in Antarctic plankton. MAAs were separated and quantified by reversed-phase high-pressure liquid chromatography (HPLC) (*87*). The quantitatively important MAAs have tentatively been identified, on the basis of co-injection analysis and online diode array spectroscopy (280 to 400 nm), as porphyra-334 (λ_{max} = 334 nm), shinorine (λ_{max} = 334 nm), palythine (λ_{max} = 320 nm), and mycosporine–glycine:valine (λ_{max} = 336 nm). The former three compounds have recently been shown to be present in intertidal diatoms, chlorophytes, and macroalgae collected near Palmer Station (*90*).
87. W. C. Dunlap and B. E. Chalker, *Coral Reefs* **5**, 155 (1986).
88. _____, J. K. Oliver, *J. Exp. Mar. Biol. Ecol.* **104**, 239 (1986).
89. J. I. Carreto, M. O. Carignan, G. Daleo, S. G. De Marco, *J. Plankton Res.* **12**, 909 (1990).
90. D. Karentz, F. S. McEuen, M. C. Land, W. C. Dunlap, *Mar. Biol.* **108**, 157 (1991).
91. K. Shibata, *Plant Cell Physiol.* **10**, 325 (1969).
92. P. M. Sivalingham, T. Ikawa, Y. Yokohama, K. Nisizawa, *Bot. Mar.* **17**, 23 (1974).
93. K. C. Smith, Ed., *The Science of Photobiology* (Plenum, New York, ed. 2, 1989).
94. B. B. Prézelin, M. M. Tilzer, O. Schofield, C. Haese, *Aquat. Sci.* **53**, 136 (1991).
95. S. Z. El-Sayed and J. T. Turner, in *Polar Oceans*, M. Dunbar, Ed. (Arctic Institute of North America, Calgary, Canada, 1977), pp. 463–503.
96. O. Holm-Hansen, S. Z. El-Sayed, G. A. Franceschini, R. L. Cuhel, in *Proceedings of the Third SCAR Symposium on Antarctic Biology*, Scientific Committee for Antarctic Research, Washington, DC, 26 to 30 August 1974, G. A. Llano, Ed. (Gulf Publishing, Houston, 1977), pp. 11–50.
97. W. O. Smith, Jr., N. K. Keene, J. C. Comiso, in *Antarctic Ocean and Resources Variability*, D. Sahrhage, Ed. (Springer-Verlag, Berlin, 1988), pp. 131–139.
98. D. G. Ainley *et al.*, *Science* **232**, 847 (1986); W. R. Fraser and D. G. Ainley, *BioScience* **36**, 258 (1986); S. J. Smith and J. Vidal, *Cont. Shelf Res.* **5**, 215 (1986); J. J. Walsh and C. P. McRoy, *ibid.*, p. 259; D. L. Garrison, K. R. Buck, G. A. Fryxell, *J. Phycol.* **23**, 564 (1987); D. G. Ainley, W. R. Fraser, K. L. Daly, in *Southern Ocean Resources & Variability*, D. Sahrhage, Ed. (Springer-Verlag, Berlin, 1988), pp. 140–146; W. O. Smith, Jr., Ed., *Polar Oceanography* (Academic Press, San Diego, CA, 1990).
99. R. C. Smith, R. R. Bidigare, B. B. Prézelin, K. S. Baker, J. M. Brooks, *Mar. Biol.* **96**, 575 (1987).
100. J. D. H. Strickland and T. R. Parsons, *A Practical Handbook of Seawater Analysis* (Fisheries Research Board of Canada, Ottawa, Canada, ed. 2, 1972).
101. W. W. Gieskes and G. W. Kraay, *Limnol. Oceanogr.* **28**, 757 (1983).
102. W. W. C. Gieskes and G. W. Kraay, *Mar. Biol.* **75**, 179 (1983).
103. R. F. C. Mantoura and C. A. Llewellyn, *Anal. Chim. Acta* **151**, 297 (1983).
104. R. R. Bidigare, M. C. Kennicutt II, J. M. Brooks, *Limnol. Oceanogr.* **30**, 432 (1985).
105. R. R. Bidigare, O. Schofield, B. B. Prézelin, *Mar. Ecol. Prog. Ser.* **56**, 177 (1989).
106. R. C. Smith, K. S. Baker, P. Dustan, *Scripps Institute of Oceanography Reference 81-17* (Visibility Laboratory, Scripps Institution of Oceanography, La Jolla, CA, 1981).
107. K. J. Waters, R. C. Smith, M. R. Lewis, *Oceanography* **3**, 18 (1990).
108. H. R. Gordon, *Appl. Opt.* **24**, 4172 (1985).
109. K. J. Voss, J. W. Nolten, G. D. Edwards, *Proc. SPIE Ocean Opt. VIII* **637**, 186 (1986).
110. Replicate seawater samples from the BOPSII were filtered (0.2 μm thick Millipore filters) immediately and frozen for subsequent nutrient analysis. All samples were measured within 4 days of collection. During sample analyses, standard calibration curves were measured every 4 hours for each nutrient (nitrate, phosphate, silicate) and were always linear. Nitrate was measured by cadmium reduction via flow-injection analysis (*99*). Phosphate and silicate were measured colorimetrically (*100*). Water samples from the BOPSII were collected

and immediately processed by HPLC, the definitive method for separating and quantifying plant pigments (*101–104*) including accessory carotenoids (*105*). Chlorophyll a concentrations from all water samples were also determined fluorometrically (*106*). Nutrient and pigment concentrations are given micromoles per liter and nanomoles per liter, respectively. Here 19′-hexanoyloxyfucoxanthin (Fig. 3I) is a diagnostic tag for *Phaeocystis* spp., which dominated the near-ice phytoplankton, and fucoxanthin (Fig. 3J) is a tag for diatoms that were found further out in the MIZ.

111. B. B. Prézelin, R. R. Bidigare, H. A. Matlick, M. Putt, B. Ver Hoven, *Mar. Biol.* **96**, 563 (1987).
112. B. B. Prézelin and H. E. Glover, *J. Plankton Res.* **13** (suppl.), 45 (1991).
113. This work was supported by NSF grants DPP 8917076 (R.C.S., B.B.P., R.R.B., and S.M.) and DPP 9002872 (D.K.) and by National Aeronautics and Space Administration grant NAGW-290-10 (R.C.S.). We acknowledge the officers and crew of the R.V. *Polar Duke*, the Antarctic Support Associates, and other Icecolors '90 team members (K. Crocker, K. Hwang, S.-H. Kang, C. Johnson, R. Jovine, A. Marotti, M. Moline, A. Morell, N. Nelson, O. Schofield, and E. Stephens). A. Krueger provided the TOMS data, C. R. Booth provided data from the NSF Division of Polar Programs UV monitoring station, and A. Torres provided the Palmer balloon O_3 data. D. Clark helped design the LUVSS instrument, which was designed and built with NSF support (DPP88-17634, R.C.S.). This is Icecolors contribution 1.

Research Article

Structural Evidence for Induced Fit as a Mechanism for Antibody-Antigen Recognition

JAMES M. RINI, URSULA SCHULZE-GAHMEN, IAN A. WILSON*

The three-dimensional structure of a specific antibody (Fab 17/9) to a peptide immunogen from influenza virus hemagglutinin [HA1(75–110)] and two independent crystal complexes of this antibody with bound peptide (Tyr^{P100}-Leu^{P108}) have been determined by x-ray crystallographic techniques at 2.0 Å, 2.9 Å, and 3.1 Å resolution, respectively. The nonapeptide antigen assumes a type I β turn in the antibody combining site and interacts primarily with the Fab hypervariable loops L3, H2, and H3. Comparison of the bound and unbound Fab structures shows that a major rearrangement in the H3 loop accompanies antigen binding. This conformational change results in the creation of a binding pocket for the β turn of the peptide, allowing Tyr^{P105} to be accommodated. The conformation of the peptide bound to the antibody shows similarity to its cognate sequence in the HA1, suggesting a possible mechanism for the cross-reactivity of this Fab with monomeric hemagglutinin. The structures of the free and antigen bound antibodies demonstrate the flexibility of the antibody combining site and provide an example of induced fit as a mechanism for antibody-antigen recognition.

FUNDAMENTAL QUESTIONS CONCERNING THE STRUCTURAL basis of antibody-antigen recognition are still largely unanswered. Although hydrogen bonding, van der Waals contacts, salt bridges, and buried surface area are of critical significance (*1*), the contribution of conformational changes in the antibody or antigen upon complexation, which may range from small changes in side-chain torsional angles to domain rearrangements, has still to be assessed. The concept of inducible fit relaxes the requirement for an exact preexisting fit between antibody and antigen. Such inducibility occurs at the expense of specificity, and hence there should be limits on the magnitude of these changes (*2*). The extent to which either the antibody or antigen changes conformation has, in fact, been much discussed (*1–6*). Both the lock-and-key (*3*) and induced fit type mechanisms (*4–6*) have been used to describe antibody-antigen recognition.

The x-ray crystal structures of a few unliganded antibodies and antigens and their respective antibody-antigen complexes have been determined and indicate that small but significant changes in both the antigen and antibody can accompany complex formation (*1, 2, 4, 5*). Complexes of Fab fragments with lysozyme and with neuraminidase (*3, 7–9*) show differences in the antigen of up to 1 to 2 Å for backbone and 2 to 4 Å for side-chain atoms, whereas the Fab′ fragment of an antibody (B13I2) to a myohemerythrin peptide and its corresponding Fab′-peptide complex show similar changes in the antibody (*5*). In addition, small but significant differences in the relative orientation of the variable heavy and light chain (V_H and V_L) domains in the Fv fragment of an antibody to lysozyme (D1.3) have been observed between the bound and unbound forms (*4*). Domain changes of a larger magnitude have been observed for an antibody (BV04-1) to single-stranded DNA (*10*).

It is not yet clear how such changes manifest themselves in terms of the specificity and selectivity of antibody antigen interactions. The potential design of antibodies with tailored specificity and catalytic properties (*11*), however, requires that we understand in structural detail the role of conformational changes in antigen recognition.

We have now determined the three-dimensional structure of Fab 17/9 from a mouse immunoglobulin [IgG2a(κ)] to a peptide, corresponding to 36 amino acid residues [HA1(75 to 110) from the influenza virus hemagglutinin (HA), in both its unliganded form and in complex with its nonamer peptide antigen (Tyr^{P100}-Asp-Val-Pro-Asp-Tyr-Ala-Ser-Leu^{P108}-amide). This antibody, Fab 17/9, is one of a panel of 21 monoclonal antibodies whose peptide binding specificity has been well characterized (*12, 13*). The minimum epitope for Fab 17/9 corresponds to the six residues from Asp^{P101} to Ala^{P106}. The nonamer peptide binds to the antibody with 50 percent inhibition at 2×10^{-8} M as determined by competition enzyme-linked immunoabsorbent assay (ELISA). The cognate peptide sequence is on the monomer surface in the HA but is located in the trimer interface and, consequently, the antibody cannot bind to the trimeric HA at physiological pH (*12, 14*). At low pH, the HA

The authors are in the Department of Molecular Biology, The Scripps Research Institute, 10666 North Torrey Pines Road, La Jolla, CA 92037. The present address of J. M. Rini is Department of Molecular and Medical Genetics, University of Toronto, Toronto, Ontario, Canada M5S 1A8.

*To whom correspondence should be addressed.